Check for updates

Archaeometry

WILEY

ORIGINAL ARTICLE OPEN ACCESS

Talc-Tempered Pottery From Bala Hissar, Kabul: An Analytical Study

Parviz Holakooei[1] | Babak Rafiei-Alavi[2] | Hafizullah Hazim[2] | Hasti Pezeshkanjalili[3] | Lara Maritan[3]

[1]Department of Objects Conservation and Archaeometry, Art University of Isfahan, Isfahan, Iran | [2]Aga Khan Cultural Service, Afghanistan | [3]Department of Geosciences, University of Padova, Padua, Italy

Correspondence: Lara Maritan (lara.maritan@unipd.it)

Received: 22 May 2026 | **Revised:** 6 July 2026 | **Accepted:** 5 August 2026

Keywords: Bala Hissar, Kabul | firing temperature | provenance | talc-schist tempered pottery

ABSTRACT

Potsherds of cooking ware excavated at Bala Hissar archaeological site in Kabul were studied using X-ray fluorescence (XRF), scanning electron microscope-energy dispersive X-ray spectrometry (SEM-EDS), Raman spectroscopy, X-ray powder diffraction (XRPD), thermogravimetric analysis (TGA) and optical microscopy. The sherds revealed to be talc-tempered associated with clinochlore, calcite, dolomite, palygorskite and chromite. It is argued that talc-schist has been most probably supplied from local talc deposits of Lalandar, located about 20 km southwest of the site. The phases identified and morphology of the crystals in the body of the potsherds suggest that they experienced firing temperatures exceeding 700°C.

1 | Introduction

Bala Hissar, Kabul, is located in the Kabul Valley along the eastern foothills of the Hindu Kush Mountains, a region widely recognised as one of the most archaeologically rich landscapes in Afghanistan. It is characterised by a high density of settlement sites and historic monuments. Today, Bala Hissar lies within the urban extent of Kabul, reflecting the long-standing interaction between the citadel and the surrounding city. The site is situated in close proximity to the Gole-Heshmatkhan wetland, a seasonal lake whose location has been shaped since the early Neolithic period. It forms part of a broader archaeological landscape that includes numerous nearby sites (such as Tappeh Maranjan, Gole Tut, Tappeh Narenj and Shivaki), many of which are associated with pre-Islamic Buddhist cultural traditions (Paiman 2013; Paiman and Filigensi 2019; Paiman and Houal 2023).

In contrast to many others of the surrounding sites, which are frequently confined to specific cultural or chronological horizons, Bala Hissar is distinguished by its remarkably long and continuous sequence of human occupation. Archaeological evidence points to sustained settlement from the pre-Islamic period through the Islamic era and into more recent centuries. This continuity makes Bala Hissar an especially valuable case study for examining long-term patterns of settlement, cultural transformation and urban development in the Kabul Valley. More broadly, it offers important insight into *longue durée* processes of human occupation across this region of Asia.

Systematic archaeological investigations at Bala Hissar have been underway since 2021 under the support of the Aga Khan Cultural Service—Afghanistan (AKCS-A) (Rafiei-Alavi et al., forthcoming). The ceramic sherds examined in this paper (Figure S1) were derived from stratigraphic Trench 3 in Zone 2. This trench constitutes one of the largest excavation units opened during 2022, 2023 and planned 2025 field seasons, extending 40 m in length, with a width varying between 4 and 6 m. Excavations in Trench 3 have revealed five principal architectural phases, further divided into several subphases, encompassing stratified deposits dated roughly between the 5th and 16th centuries CE.

Phases 5 and 4 are attributed to the pre-Islamic period, while Phases 3 through 1 correspond to successive stages of the

This is an open access article under the terms of the Creative Commons Attribution License, which permits use, distribution and reproduction in any medium, provided the original work is properly cited.

© 2026 The Author(s). *Archaeometry* published by John Wiley & Sons Ltd on behalf of University of Oxford.

Islamic era. Although the stratigraphic sequence in Trench 3 does not extend earlier than the late antique period, investigations in other areas of Bala Hissar—an archaeological complex covering nearly 50 ha—have identified earlier occupation levels dating back to approximately the first century BCE. These findings demonstrate that the broader occupational history of the site significantly precedes the sequence documented in Trench 3.

The talc-tempered pottery assemblage from Bala Hissar consists primarily of simple, handmade wares that display a limited yet consistent range of forms. These include cooking pots, lids that can likely be associated with these vessels and a smaller number of bowls (Figure S2). In terms of both technology and function, this pottery appears to have been produced for everyday domestic use rather than for display or elite consumption.

Many of the vessels bear clear evidence of exposure to fire, such as surface discoloration, thermal alteration and the presence of soot (Table S1). These traces point to their regular use in food preparation and cooking, most probably within a household setting. The dominance of utilitarian forms, together with signs of repeated heating, highlights the role of this pottery in routine culinary practices.

Although the ceramics are generally plain and only minimally finished, some examples show modest decorative treatment that introduces a degree of visual variation. This includes the application of red or orange pigments as well as incised decoration, most often in the form of simple geometric patterns (Table S1). Such features appear more frequently on lids, suggesting that decoration may have been selectively applied to particular vessel elements. Taken together, the talc-tempered pottery from Bala Hissar reflects a largely functional ceramic tradition, with occasional attention to aesthetic detail, embedded in the everyday domestic life of its users (Figure S2).

This pottery type is found mainly in Occupational Phases 3 and 2, with a noticeably higher concentration in Phase 3. In Trench 3 alone, approximately 1000 sherds were recovered from Phase 3, compared to around 600 from Phase 2. It should be noted, however, that these numbers represent only a small proportion of the overall ceramic assemblage from the trench. This suggests that talc-tempered pottery formed a relatively minor, though still diagnostically important, component of the material record.

The difference in quantity between the two phases indicates that the use of talc-tempered pottery likely reached its peak during Phase 3, followed by a clear decline in Phase 2. In chronological terms, Phase 3 can be dated to approximately 1200–1300 CE, while Phase 2 corresponds to the period between about 1400 and 1500 CE. On this basis, the use of this ceramic type appears to span roughly three to four centuries, from the 13th to the 16th century CE. At the same time, the concentration of material in Phase 3 suggests that its main period of use falls in the earlier part of this range.

This work focuses on the multi-analytical characterisation of the talc-temper pottery, as whole and of its inclusions, to define possible changes in the production technology over the different phases.

2 | Materials and Methods

To build upon the analytical framework outlined above, six samples (Figure S1) were selected to be examined using a multi-analytical approach. These undiagnostic body sherds, drawn from both Phase 3 and Phase 2 contexts, were intended to represent a broad cross-section of this ceramic type. At a macroscopic level, the fabrics are notably soft and display a slightly soapy texture characteristic of talc-tempered wares. This makes the surfaces highly susceptible to abrasion; they can be easily scratched with a fingernail. The sherds also show relatively low mechanical strength, as some can be broken with minimal force, occasionally even by hand. These qualities distinguish the pottery technologically and prompted further investigation into its composition and methods of manufacture. The selected samples were chosen to provide a representative subset of the assemblage, supporting more reliable observations on the characteristics of this ceramic tradition.

Four sherds from which sufficient amounts of powdered samples could be collected in order to be analysed by wavelength-dispersive X-ray fluorescence (WD-XRF) were selected to acquire the compositional data from the bulk of the bodies. Major and minor element oxides (SiO_2, TiO_2, Al_2O_3, Fe_2O_3, MnO, MgO, CaO, Na_2O, K_2O and P_2O_5, expressed in weight percent, wt%) together with trace elements (Sc, V, Cr Co, Ni, Cu, Zn, Ga, Rb, Sr., Y, Zr, Nb, Ba, La, Ce, Nd, Pb, Th and U expressed in part per million, ppm) were determined using a sequential WDS Panalytical Zetium spectrometer (Rh tube with 2.4 kW as maximum power). Glass beads of samples were prepared by mixing the sample calcinated powder with $Li_2B_4O_7$ in a 1:10 dilution ratio in order to reduce the matrix effect on the quantification of elements.

Due to small amount of sample could be collected from the sherds, two of them were not possible to be analysed by WD-XRF. Therefore, an ARTAX 200 energy dispersive XRF (ED-XRF) device from Bruker equipped with an Mo X-ray tube was used to acquire compositional data from the polished cross-sections of minute samples. The ED-XRF spectra were collected at 25 kV and 1000 μA for 60 s employing a 1-mm collimator. In order to check and to correct the quantitative data obtained by Python multichannel analyser (PyMCA), GSR-3 (basalt), JGb-2 (gabbro), NIM P (pyroxenite), Sco 1 (serpentinite) and UB-N (cody shale) were used as certified reference materials (CRMs). The data acquired CRMs together with the uncertainty and relative error of the measurements have been published by Holakooei et al. (2026).

An XMF-104 micro-X-ray fluorescence (μ-XRF) device from Unisantis (Switzerland) equipped with an Amptek Si-PIN detector and an X-ray Tube (Mo anode) was used for analysing large crystals embedded in the bodies (the large crystals were easily observed with naked eye as can be seen in Figure S1). The advantage of this device was that it was equipped with a Kumakhov polycapillary lens which focused the X-ray beam in a spot about 80 μm so that single crystals could be analysed with

14754754, 0, Downloaded from https://onlinelibrary.wiley.com/doi/10.1111/arcm.70203 by Cochraneltalia, Wiley Online Library on [09/09/2026]. See the Terms and Conditions (https://onlinelibrary.wiley.com/terms-and-conditions) on Wiley Online Library for rules of use; OA articles are governed by the applicable Creative Commons License

this approach. The measurements were performed at 35 kV and 500 mA for 5 min in air. It should be noted that the μ-XRF measurements were performed on the cross-section of the samples embedded in epoxy resin and polished with soft abrasive papers up to 5000 grid number. The quantification procedure was based on analysing the CRMs previously studied and published by Holakooei et al. (2024).

All the samples were cut by a sharp scalpel, embedded in epoxy resin, and the cross-sections were polished and observed under polarised light microscope (Primotech, Zeiss Co. Ltd., coupled with Axicam digital camera for image acquisition). The petrographic analysis was carried out following the procedure and terminology of Quinn (2022) and Maritan (2024).

The samples were also analysed by scanning electron microscope (SEM) using a Tescan Solaris field emission FE-SEM equipped with an Oxford Instrument energy dispersive spectrometer (EDS). Carbon-coated polished sections were analysed at ultra-high resolution both in back scattered electron (BSE) and secondary electron (SE) at 15 keV and 3 nA–300 pA. A Quanta FEG-450A FE-SEM from FEI was also used to semi-quantitatively analyse the cross sections of the samples and to create X-ray elemental maps of elements coating them with Au and analysing under high vacuum at 25 kV.

Micro-Raman (μ-Raman) spectroscopy was also used to study the blackened surface of the potsherds and the large crystals in the bodies, using a Takram DL G-100 spectrometer (supplied by Teksan, Iran) operating with two laser lines (i.e., 532 and 785 nm) and equipped with four gratings (600, 1200, 1800 and 2400 groove/mm), which provided a spectral resolution between 1 and 12 cm^{-1}. Each spectrum was obtained by accumulating and averaging 5 spectra with a 10-s acquisition time.

The bulk mineralogical analysis of the samples was performed by X-ray powder diffraction (XRPD) using a Bruker D8 Advance X-ray Diffractometer, with Cu-Kα radiation, 40 kV and 30 mA and a step size of 1°/2θ/min in the 4°–70° 2θ range. Quantitative phase analyses were carried out based on the ICDD-PDF2 and COD databases for X-ray diffraction powder data, and the phases were quantitatively estimated using Maud software package.

Finally, thermogravimetric (TGA) analysis and their derivative curves (DTG) were obtained from about 15 mg of the same powder with a LABSYS evo instrument from SETARAM in static air with a heating rate of 10°C min^{-1} from room temperature up to 1000°C, using alumina crucible with fused alumina powder as the reference standard.

3 | Results

3.1 | Microscopic Observations

From the microscopic point of view, the samples are characterised by very abundant (30%–50%) elongated fragments of talc-schist (Figure 1a). They occur both with fine and coarse size, from few tens of microns up to 2 mm, being rounded or subrounded in shape. They have a closed spaced-related distribution, showing therefore a very dense packing in the ceramic groundmass. Talc crystals appear colourless and with the typical interference colour up to the third order (Figure 1b). They are occasionally associated, within the same fragment, also to crystals of chlorite having a brownish colour in plain-polarised light and being optically inactive in crossed-polarised light (Figure 1c), indicating that the mineral underwent at least partial decomposition. Talc fragments also contain opaque minerals (Figure 1d) and are occasionally associated to calcite crystals (Figure 1e) or to tremolite (Figure 1f), this latest showing the typical very elongate habit and high relief. Talc-schists are the prevalent inclusion type, associated to opaque minerals, often with a euhedral habit (isodiametric) or rounded in shape. Rarely crystals of calcite and dolomite can also be observed.

The matrix is optically inactive, and the porosity is represented by large vughs and channels, reaching also the millimetric dimension. The study samples show analogous petrographic features, and the difference among them is related to slightly different inclusion content and grain size, but they represent the variation within an almost standardised production recipe for which a clayey material was collected very close to talc outcrops.

The observation of the samples under FE-SEM clearly indicates that the fragments of talc are very abundant in the ceramic body and occur with size down to some tens of microns (Figure 2a,b). They are randomly oriented, so that in some cases, it is possible to see their basal face (001) (Figure 2c,d), while in others, the various flakes are intersected along the [001] direction (Figure 3a,b). Talc flakes do not show any trace of decomposition, such as the formation of bridging between flakes or along the cleavage plains, nor the crystallisation of high temperature phases, such as enstatite (Figure 3c). In some inclusions, talc crystals are locally associated with chlorite (Mg-rich chlorite) and oxides, such as magnetite (Figure 3d) and chromite.

Focusing on the thermal stability of other mineral phases present in the samples, it can be seen under the microscope that both chlorite and biotite have lost the characteristic aspect both in plain- and crossed-polarised light. At the FE-SEM, flakes of chlorite, micro-chemically characterised by a high content of magnesium and therefore being close to the clinochlore end-member, are characterised by incipient decomposition, with local development of bridging between the cleavage planes (Figure 4a,b). The same can be observed in some crystals of biotite (Figure 4c,d), in which the cleavage planes (001) seem to open and between them a melted phase developed forming intense bridging structure. Calcite is, in most of the cases, well-preserved with only few situations in which pores, rounded in shape and of the size of few microns, appear along the cleavage system (Figure 2a).

3.2 | Chemistry of the Sherds

The bulk chemical composition of the bodies (Table S2) demonstrated that they are rich in silicon (SiO_2), magnesium (MgO), calcium (CaO) and iron (Fe_2O_3) together with traces

14754754, 0, Downloaded from https://onlinelibrary.wiley.com/doi/10.1111/arcm.70203 by Cochraneltalia, Wiley Online Library on [09/09/2026]. See the Terms and Conditions (https://onlinelibrary.wiley.com/terms-and-conditions) on Wiley Online Library for rules of use; OA articles are governed by the applicable Creative Commons License

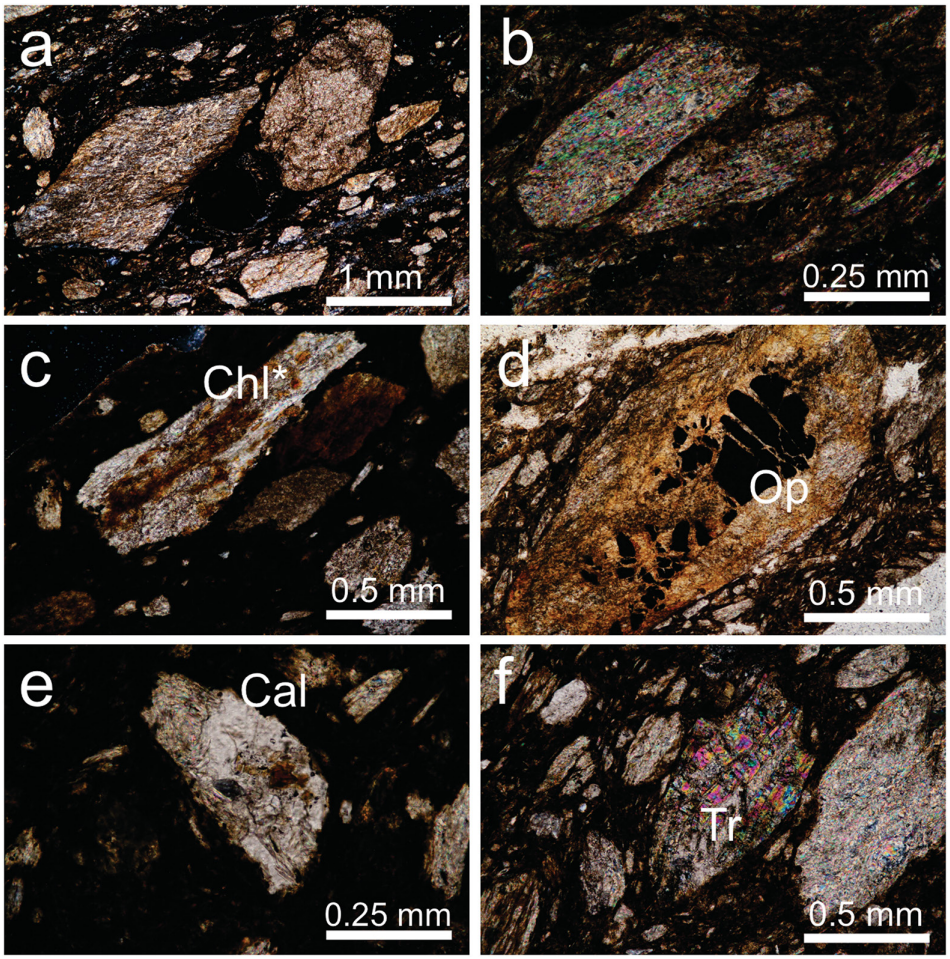


FIGURE 1 | Photomicrographs in plain-polarised light (PPL) and crossed-polarised light (XPL) of (a) talc-schist fragments (Sample 1, PPL) showing a very dense packing within the ceramic body; (b) talc-schist inclusions with the typical interference colours (Sample 3, XPL); (c) talc-schist bearing chlorite crystals which underwent partial decomposition and do not show the characteristic interference colour, but appear brownish (Sample 2, XPL); (d) talc-schist with decomposed chlorite (brownish also in PPL) and large opaque minerals (sample 3); (e) talc-schist with calcite (sample 5, XPL); (f) talc-schist with tremolite (sample 5, XPL). Abbreviations: Cal, calcite; Chl*, partially decomposed chlorite (not interference colour in XPL); Op, opaque minerals; Tr, tremolite.

of nickel (Ni) and chromium (Cr). The high magnesium and low calcium content of the samples rule out the occurrence of dolomite and instead suggest that talc is a main component in the samples.

The body of Samples 2 and 4 is slightly different from the others in terms of higher CaO content. The occurrence of Cr and Ni was of interest as they are elements associated with mafic rocks such as talc and maybe indicative of the provenance of the original rock used as temper in the bodies. μ-XRF data on the talc crystals (Table S3) demonstrated that the Ni/Cr in Samples 1 and 3 is fairly similar and different from that in Sample 2.

As a further step, the amount of trace elements (i.e., Fe, Cr, Ni, Zn and Cu) and their correlation in the talc crystals were investigated using μ-XRF quantitative data. As Figure S3 (Supporting Information) demonstrates, manganese (Mn) and Fe were associated in all talc crystals in the potsherds under study. Similarly, Fe and Ni showed a relatively high correlation in the talc crystals suggesting that the source of Ni and Mn in the talc crystals is the same.

These elements are in fact vicariant of Mg, and therefore, they can enter the crystal lattice of talc (Bloise et al. 2026) having also important implications on the sintering effect of ceramic materials but only for those fired at very high temperature (above 1100°C).

However, while Zn and Ni showed to be highly correlated in Sample 2, this pair showed low correlation in other samples. A particular negative correlation was also observed between Cu and Zn in Samples 1 and 3. The correlation between the above-mentioned pairs of elements suggests that talc crystals in Sample 2 may represent different chemistry or possibly a different origin.

X-ray elemental maps (Figure S4) acquired from the cross-section of the samples showed that Cr is not associated with Ni and, instead, seems to be correlated with Al. The association of Cr and Mg may not be properly observed in the X-ray elemental maps as the matrix is highly rich in Mg. The Cr-bearing particles, as SEM-EDS data showed, are rich in Mg and Fe suggesting chromite as an inclusion in the talc crystals, and Cr# is fairly similar for the chromite particles analysed by SEM-EDS (Table S4).

14754754, 0, Downloaded from https://onlinelibrary.wiley.com/doi/10.1111/arcm.70203 by CochraneItalia, Wiley Online Library on [09/09/2026]. See the Terms and Conditions (https://onlinelibrary.wiley.com/terms-and-conditions) on Wiley Online Library for rules of use; OA articles are governed by the applicable Creative Commons License

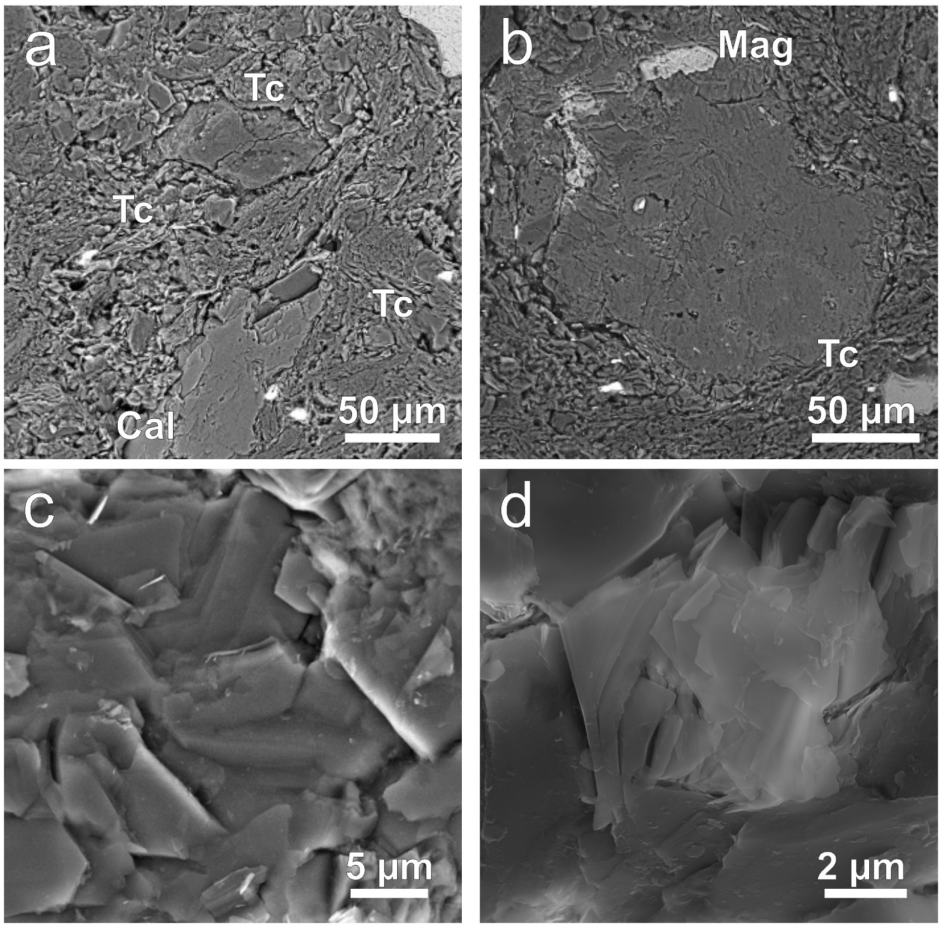


FIGURE 2 | FE-SEM images taken in back scattered electrons (BSE) or in secondary electrons (SE) of (a, b) ceramic body with talc inclusions with variable size from hundreds to down to some tens of microns, sometimes containing also crystals of chromite and occasionally associated to inclusions of calcite; (c, d) basal sections (001) of crystals of talc; (e, f) section along the [001] direction of crystals of talc; (g) detail of crystals of talc which do not show any trace of decomposition; (h) euhedral crystals of magnetite into a talc fragment. Abbreviations: Cal, calcite; Mag, magnetite; Tc, talc.

3.3 | Mineralogical Composition of the Sherds

The XRPD patterns on the powdered samples showed that the samples contain talc (Reference code: 01-073-0147), clinochlore (Reference code: 01-079-1270), palygorskite (Reference code: 01-082-1873), quartz (Reference code: 96-101-1177), dolomite (Reference code: 96-900-3519) and calcite (Reference code: 01-085-1108) (Figure S5; raw data available as Data S1). All potsherds contained more than 75 wt% of talc (Table S5). All the XRPD patterns showed a broad band from 5° to 15 2θ°, which may be related to noncrystalline phases in the bodies, comprising both the amorphous phase developed during firing (mainly from the decomposition of pristine phyllosilicates) and organic compounds. Since these sherds are from potteries mainly used for cooking purposes, organic residues can be expected to partially fill the porosity of the bodies, therefore contributing to the amorphous content of the powdered sample.

Principal component analysis (PCA) and hierarchical clustering analysis (HCA), which were performed to define possible similarities between the XRPD patterns of the samples (Figure S6), show that while Samples 1 and 3 are grouped in a cluster due to the fairly same amounts of talc, dolomite and clinochlore phases, the rest of the samples represent different amounts of these phases. This is also evident in the amount of the phases measured from these two samples (Table S5) and also from a simple inspection of the patterns of Figure S5 (Supporting Information). However, it must be emphasised that almost all the samples represented the same chemistry and phase composition. In summary, the phases detected in XRPD patterns were entirely consistent with those observed through microscopic analysis except for those occurring in low quantity (i.e., chromite, palygorskite and tremolite), which were below the observation/detection limit of either these approaches.

TGA data (raw data available as Data S1) shed further light on the mineralogical associations of samples. As Figure 5 demonstrates, all the powdered samples from the sherds showed a lower than 0.5 wt% loss of weight at about 100°C related to the adsorbed water. In addition, all the samples revealed about 4 wt% weight loss at 880°C, which is linked to the decomposition of talc. This is well consistent with about 80 wt% talc measured from the XRPD patterns (Table S5). Also, a loss of weight was observed for all the samples at about 800°C–830°C, which may be related to Mg-Fe chlorite and clinochlore (Földvári 2011). This loss of weight is about 1 wt% and in line with about 3–7 wt% from clinochlore measured

14754754, 0, Downloaded from https://onlinelibrary.wiley.com/doi/10.1111/arcm.70203 by Cochraneltalia, Wiley Online Library on [09/09/2026]. See the Terms and Conditions (https://onlinelibrary.wiley.com/terms-and-conditions) on Wiley Online Library for rules of use; OA articles are governed by the applicable Creative Commons License

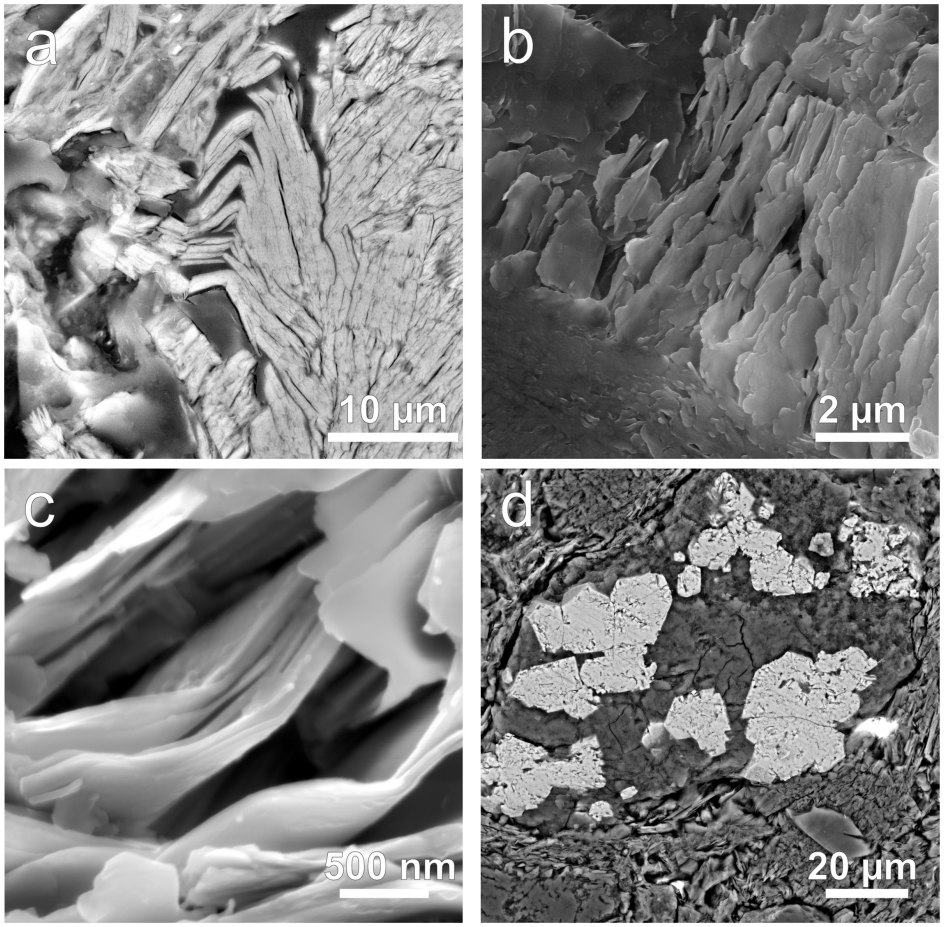


FIGURE 3 | FE-SEM images taken in back scattered electrons (BSE) (a, d) or in secondary electrons (SE) (b, c) of (a, b) section along the [001] direction of crystals of talc; (c) detail of crystals of talc which does not show any trace of decomposition; (d) euhedral crystals of magnetite (light grey colour) into a talc fragment.

from the samples. It should be noted that since the decomposition temperature of chlorite is slightly lower (~750°C), the weight loss at about 800°C–830°C may also be due to the fast heating of the TGA experiment. As an exception, Sample 6 revealed a loss of weight of about 2 wt% in this range, which is related to the higher clinochlore embedded in this sample. In fact, about 2 wt% loss was entirely expected from 15 wt% from clinochlore in this sample measured by XRPD. Moreover, loss of weight occurred from 700°C to 800°C in Samples 1–4 can be related to carbonates (i.e., calcite and dolomite) in the bodies (Table S5). A peculiar loss of weight was observed from 500°C to 530°C in Sample 2, which may be related to the decomposition of organic material.

Another issue that should be highlighted is that all the samples revealed about 1% (from 0.7 to 1.5 wt%) weight of loss at temperatures lower than 500°C, which can be attributed to the decomposition of the organic materials remained in the bodies as a consequence of cooking. In addition, the quantity of palygoskite was lower than the limit to show a significant loss of weight in the TGA curves. The total loss on ignition (LOI) measured from the TGA thermograms of the samples was fairly comparable with the theoretical LOI calculated based on the phases measured from the XRPD patterns (Table S6). The slight difference between the theoretical and experimental LOI may be related to the intrinsic error in the quantification of the phases or can be linked with the organic residue in the bodies which cannot be measured by the approach adopted in this study. In fact, the broad peak between 5° and 15° in the XRPD patterns can be most probably related to an organic component, whose presence was attested by TGA analysis.

Raman study on the large crystals embedded in the bodies (raw data available as Data S1) further supported the occurrence of talc with the Raman bands at 195, 291, 363, 432 and 676 cm^{-1} consistent with those from mineral talc, where the apfu for Mg was calculated, as suggested by Aspiotis et al. (2023), to be three perfectly match with mineral talc. Raman signals from the black crusts, apart from the Raman bands connected to talc, showed two broad bands centred at 1382 and 1597 cm^{-1} (Figure S7) which are from carbon black. Here, the band at 1382 cm^{-1} is attributed to stretching vibrations in the planar graphite structure (G band) and that centred at 1597 cm^{-1} is driven from the defects of graphite structure or disorder band (D band). The ratio between the full width at half maximum (FWHM) for the D and G bands (i.e., I_G/I_D) was calculated 0.7. The centres of the D and G bands and the I_G/I_D ratio suggest that a black earth occurs on the potsherds (Tomasini et al. 2012).

14754754, 0, Downloaded from https://onlinelibrary.wiley.com/doi/10.1111/arcm.70203 by CochraneItalia, Wiley Online Library on [09/09/2026]. See the Terms and Conditions (https://onlinelibrary.wiley.com/terms-and-conditions) on Wiley Online Library for rules of use; OA articles are governed by the applicable Creative Commons License

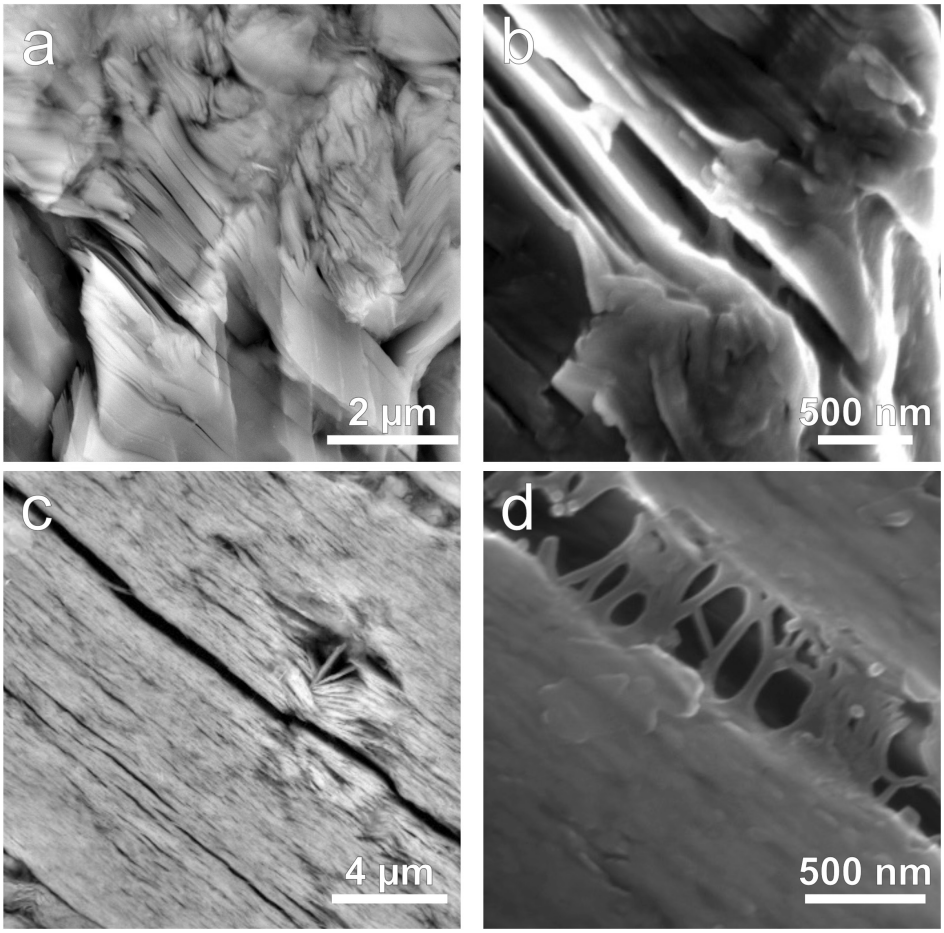


FIGURE 4 | FE-SEM images taken in back scattered electrons (BSE) or in secondary electrons (SE) of (a, b) flakes of chlorite showing incipient decomposition as attested by the separation of the flakes along the [001] direction and the formation of bridging; (c, d) flakes of biotite showing incipient decomposition with the separation of flakes along the [001] direction and the formation of bridging.

4 | Discussion

4.1 | Talc-Tempered Pottery of Bala Hissar in Context

Talc-tempered pottery has been reported across a wide geographical range, from the Far East in Korea and Japan (Takesue 2011; Choi et al. 2017) and Puma in Tibet (Reedy et al. 2017) to the far western lands of southern (Carlevato 1988) and northern America (Ownby et al. 2004); from the Urals (Anthony 2007; Johnson 2016) down to southern Arabia (Blakely and Glanzman 1996; Porter 2018; Zampierin et al. 2024) and Africa (Wilson 1973). The chronological span of talc-tempered pottery use is similarly vast. It ranges from the fifth-millennium BC examples in southwestern Poland (Borowski et al. 2015) and Bronze Age steatite-tempered ceramics from the southern Urals (Johnson 2016), Scotland (Neighbour et al. 1998; Downes 2012), Syria (Duistermaat 2017) and Finland (Ikaheimo and Panttila 2002), to Sasanian and Islamic talc-tempered ceramics in Iraq (Potts et al. 2018), modern African (Wilson 1973; Lyons et al. 2018) and Tibetan (Reedy et al. 2017) ceramics incorporating talc. Talc-schist has also been reported as a shiny golden slip on the bodies of ceramics (Maritan et al. 2018), from a context geographically and chronologically comparable to the talc-tempered sherds from Bala Hissar, Kabul.

As this study suggested by the occurrence of carbon black (soot) on the body of the potsherds, these wares have been most certainly used for cooking purposes. In line with this observation, almost exclusively the use of talc-tempered pottery is linked with cooking and kitchen utensils in literature. It is argued that the ceramic pots compared a cheap price with respect to the metal kitchen wares (Gascoigne 2013). In fact, talc-tempered potteries have been advocated to be used as cooking ware due to several reasons including their low coefficient of thermal expansion, insulating properties and high latent heat retention (Borowski et al. 2015), which make them suitable for heating and cooling.

According to the Islamic sources of cook-books, potteries or talc-schist objects are not subject to multiple use as a result of their improper cleaning after cracking and fixing and their low price, which makes them feasible to be replaced by new ones (Gascoigne 2013). Although the repair of certain types of pottery after breakage appears to have been a common practice at Bala Hissar, talc-tempered pottery is difficult to repair because its fractured edges are irregular and uneven, making accurate reassembly challenging—particularly if the vessel was intended to hold liquids. In this instance, only a single sherd bearing a perforated hole at the rim has been identified, suggesting that the vessel was repaired following damage. This evidence implies that the repair was limited to the rim, while the remainder of the vessel likely remained intact. There is however evidence of several

14754754, 0, Downloaded from https://onlinelibrary.wiley.com/doi/10.1111/arcm.70203 by CochraneItalia, Wiley Online Library on [09/09/2026]. See the Terms and Conditions (https://onlinelibrary.wiley.com/terms-and-conditions) on Wiley Online Library for rules of use; OA articles are governed by the applicable Creative Commons License

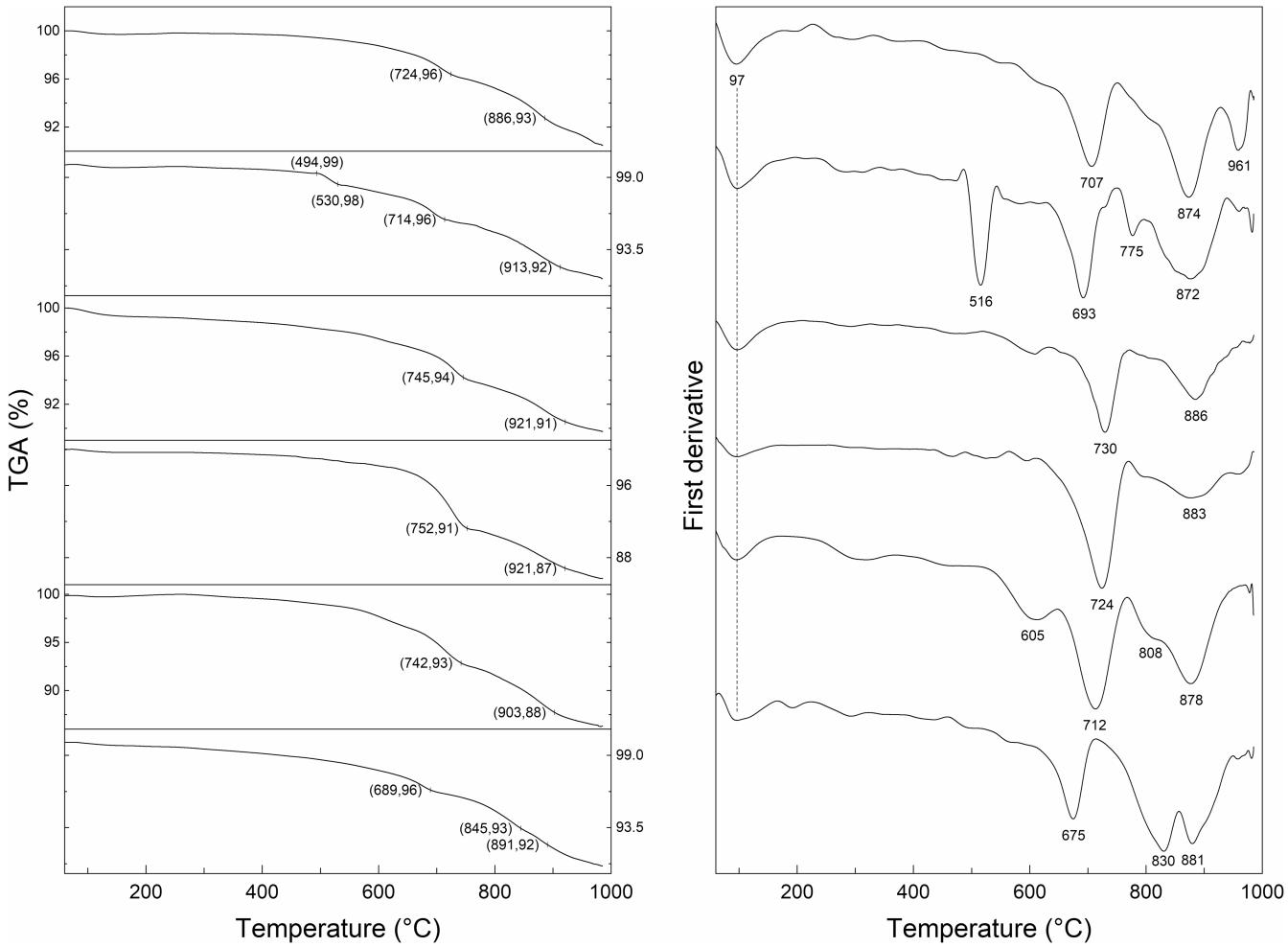


FIGURE 5 | (left) TGA thermograms (the temperature and percent of weight are shown in parentheses) and (right) their first derivative curves of Samples 1–6 from top to bottom, respectively.

phases of repair on a steatite ware from Siraf, southern Iran, which is in favour multiple use of such objects (Jennings 2018). Ownby et al. (2004) have shown that microstructure of talc-schist opens as a result of firing and, consequently, can preserve food residue in its structure with respect to the other wares made of stone and metal. Therefore, a future study may be conducted to study the organic residue preserved in the body of the potsherds under study.

4.2 | Provenance of the Shards

It is suggested that the potteries used for culinary purposes are mainly local products. In fact, the talc-tempered potteries, due to their fragility, are not items of trade and long transportation (Ikaheimo and Panttila 2002). Although many studies have supported this claim, evidence against it is also reported which shows long-distance exchange and circulation of talc-tempered potteries over centuries (e.g., Kaiser 1989; Duistermaat 2017). Therefore, a discussion about the provenance of the objects under study may be helpful.

The largest talc sources in Afghanistan are located in Nangarhar province, where Achin talc-magnesite and the Gunday talc deposits are found. While the Gunday deposit consists of talc lenses and pods and outcrops between Proterozoic marble and gabbro-diabase, the Achin talc-magnesite deposit is found exposed in the Proterozoic marble intruded by andesite porphyry and diabase porphyry dykes. Here, the talc veins contain steatite, dolomite, magnesite, quartz and calcite. Both deposits are hydrothermal and Eocene in age (ESCAP 1995) and are associated with magnesite (Orris and Bliss 2002) with no occurrence of chromite (Cocker 2018). Apart from the talc deposits in Nangarhar, there is Ferenjal talc source in Parwan Province which occurs in serpentinite containing chrysotile veinlets. This occurrence is situated at the contact between a serpentinised plug and Lower Carboniferous schist (Sutphin et al. 2007) and is mainly associated with chrysotile (Orris and Bliss 2002).

The nearest talc deposit to Bala Hissar archaeological site is located in Lalandar, Charasyab District, in Kabul (Figure 6). The igneous activity in the Kabul structural block is marked by the ultrabasic rocks, which incorporate harzburgite, lherzolite, dunite, pyroxenite and serpentine aged to the Lower Eocene and associated with chromite, asbestos and talc mineralization (ESCAP 1995). Here, talc occurs in Lalandar area located near the contact between Eocene ultramafic bodies and interbedded slate and marbled limestone of Late Permian age. This

14754754, 0, Downloaded from https://onlinelibrary.wiley.com/doi/10.1111/arcm.70203 by CochraneItalia, Wiley Online Library on [09/09/2026]. See the Terms and Conditions (https://onlinelibrary.wiley.com/terms-and-conditions) on Wiley Online Library for rules of use; OA articles are governed by the applicable Creative Commons License

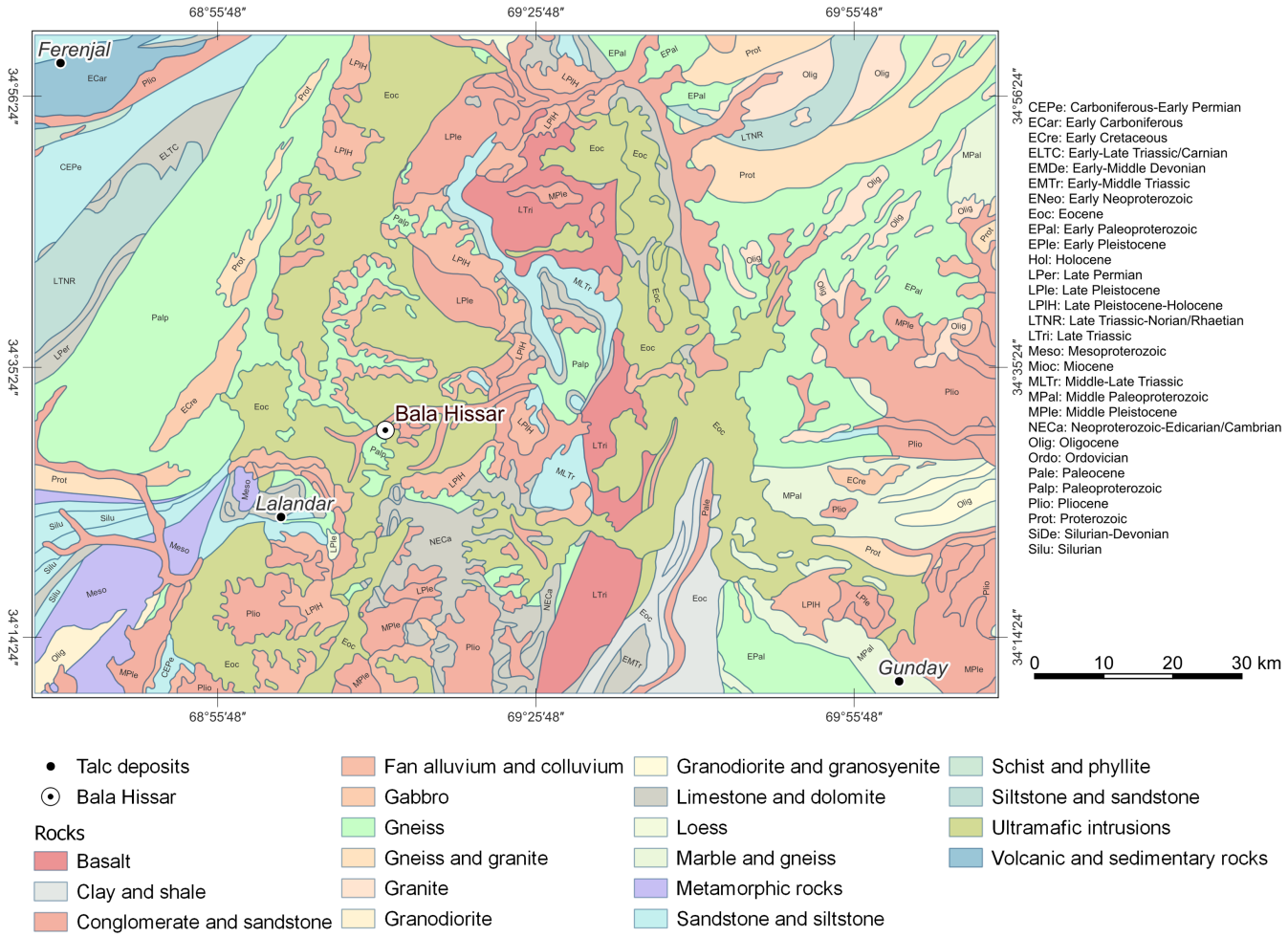


FIGURE 6 | Geologic map of the area around Bala Hissar archaeological site (reproduced after Orris and Bliss 2002).

occurrence consists of talc-bearing zones and lenses of talc exploited by local residents (Sutphin et al. 2007). In addition, talc mine in Lalandar area contains chromite (Renaud 2024).

A number of clues suggest that the talc-tempered pottery found at Bala Hissar is most probably locally produced. The vicinity of the Lalandar talc deposit to Bala Hissar (Figure 6), few kilometres apart, and the occurrence of chromite in the talc-schist inclusions as proved by SEM-EDS are in favour of this claim. In addition, the trace elements (Cr, Ni, Zn and Mn) associated with talc-schist crushed pieces (Table S3) and the bodies acquired by WD-XRF and ED-XRF (Table S2) are significantly different from those published from the talc deposits of Nangarhar (Tahir et al. 2018; Yousufzai et al. 2020). Furthermore, the absence of magnesite and chrysotile, as the main associated minerals with talc in the Nangarhar and Parwan talc deposits, respectively, in the samples under study rules out the use of talc-schist from these regions.

The question of provenance may however not be straightforward as explained. As Porter (2018) has suggested, the by-products of steatite carving and steatite dust could have been transported for use in pottery production. In other words, some crushed steatite as by-product steatite carving could have been imported into a region where it is mixed with clay in order to manufacture a final product. Therefore, caution must be taken into account that although the talc-schist found in a potsherd may have been supplied from Lalandar, the whole potsherd may have been made somewhere else and reimported to the region.

4.3 | Firing Regime

The firing regime of the potsherds is not only limited to the firing process that the potsherds have undergone in the kiln but also expanded to the heating of the pots in the course of several or at least one cooking cycle. The following depiction of the firing regime is therefore an overall estimation of firing temperature that the potteries under study have undergone rather than the equivalent firing temperature as suggested by Tite (1995). The well-preserved crystals of talc, with the typical interference colours and without any evidence of partial melting (bridging) or newly formed phases, as well as the clear diffraction peaks in XRPD pattern, indicate that talc did not undergo breakdown of the crystal lattice, and therefore, the potsherds were fired at temperatures below 800°C. The experimental firing of talc-schist (Maritan et al. 2018), in fact, showed that talc decomposes from 800°C and then crystallises enstatite and forsterite.

As for clinochlore, the presence of this phase in the XRPD patterns of all the samples, despite its low concentration, indicates that it did not decompose during firing at least not completely.

14754754, 0, Downloaded from https://onlinelibrary.wiley.com/doi/10.1111/arcm.70203 by CochraneItalia, Wiley Online Library on [09/09/2026]. See the Terms and Conditions (https://onlinelibrary.wiley.com/terms-and-conditions) on Wiley Online Library for rules of use; OA articles are governed by the applicable Creative Commons License

The microstructural features, especially the incipient development of bridging (not in large extent), attest that it experienced firing temperature lower than its decomposition that, considering its high content of magnesium, should have not exceed 800°C. Literature data (Steudel et al. 2016), in fact, report that magnesium-rich chlorite decomposes at higher temperature than iron-rich chlorite, this latter decomposing at temperature lower than 650°C–700°C (Maritan et al. 2006; Gliozzo 2020). As for biotite, despite it tends to decompose at temperature exceeding 850°C (Riccardi et al. 1999), it can have a different thermal behaviour according to its grain size (Travé Allepuz 2021). Therefore, since in the studied samples biotite flakes are smaller than 250 μm, the intense transformation could have occurred at lower temperature.

Finally, the well-preserved crystal of calcite, only occasionally showing micropores for the incipient decarbonation along the cleavage system, indicates that the ceramic experienced firing temperature below or close to 700°C (Tenconi et al. 2016; Maritan et al. 2021). This firing temperature is also in agreement with the occurrence of dolomite in some samples, which tend to decompose at temperatures around 700°C–750°C, according to its grain size (Nodari et al. 2007; Gliozzo 2020). Therefore, despite minor differences both within and between samples, the mineral associations, comprising only minerals related to the used raw materials and none newly formed (high temperature) ones, as well as the microstructural features observed in phyllosilicates and carbonates, both indicate that the samples experienced firing at temperatures close to 700°C.

5 | Conclusions

A multi-analytical approach indicates that the talc-tempered pottery from Bala Hissar was produced using locally sourced materials, readily available for quarrying and use. The low firing temperatures, simple designs and uncomplicated mineralogical profile point to a relatively modest manufacturing process that could be carried out without specialised knowledge or the sophisticated techniques required for high-quality ceramics. This pottery type, similar to other talc-schist tempered wares found worldwide, appears to have been widely used as kitchen utensils, likely due to its insulating and thermal properties. It should be emphasised that the thermal history of these potteries is difficult to reconstruct with certainty, given their repeated use as cooking utensils. In addition to the initial firing during production, kitchenware is frequently reheated (often many times) for cooking purposes, making the interpretation of their thermal profiles far from straightforward. Lastly, the TGA data presented in this study support the hypothesis that the potsherds incorporate organic materials within their body. Future research should therefore focus on extracting and identifying these organic residues, which are likely trapped in the porous bodies of the sherds, to gain insights into food consumption patterns and culinary habits in Kabul during late antiquity.

Acknowledgements

Carmela Vaccaro and Renzo Tassinari from the University of Ferrara, Italy, are thanked for providing access to ED-XRF and CRMs. As part of a large-scale conservation project, led by the Aga Khan Cultural Services, Afghanistan (AKCSA) and funded by the ALIPH Foundation, field archaeological investigations were initially carried out at the Bala Hissar Citadel between 2019–2021 in cooperation with the French Archaeological Delegation for Afghanistan (DAFA). Subsequently, between 2022–2026, archaeology was conducted directly by the AKCSA, led by Babak Rafiei-Alavi and a local team of Afghan archaeologists, working in coordination with the Archaeological Institute of Afghanistan (AIA) of the Ministry of Information and Culture. Open access publishing facilitated by Universita degli Studi di Padova, as part of the Wiley - CRUI-CARE agreement.

Data Availability Statement

The data that support the findings of this study are available in the Supporting Information of this article.

Peer Review

For transparency, the peer review documents associated with this article are available at https://doi.org/10.1111/arcm.70203.

References

Anthony, D. W. 2007. *The Horse, the Wheel, and Language: How Bronze-Age Riders From the Eurasian Steppes Shaped the Modern World*. Princeton University Press.

Aspiotis, S., J. Schlüter, F. Hildebrandt, and B. Mihailova. 2023. "Raman Spectroscopy for Crystallochemical Analysis of Mg-Rich Layered Silicates: Serpentine and Talc." *Journal of Raman Specroscopy* 54, no. 12: 1502–1516. https://doi.org/10.1002/jrs.6601.

Blakely, J., and W. Glanzman. 1996. "From Clay to Stone? Cooking Bowls of South Arabia." In *Retrieving the Past: Essays on Archaeological Research and Methodology in Honor of Gus W. Van Beek*, edited by J. D. Seger, 3–26. Eisenbrauns.

Bloise, A., F. Parisi, M. F. La Russa, et al. 2026. "Hydrothermal Synthesis of Pure Talc, Mn and Ni-Doped Talc and Their Impact on Stoneware Tiles Sintering." *Applied Clay Science* 290: 108271. https://doi.org/10.1016/j.clay.2026.108271.

Borowski, M. P., M. Furmanek, K. Czarniak, and P. Gunia. 2015. "Steatite-Tempered Pottery of the Stroke Ornamented Ware Culture From Silesia (SW Poland): A Neolithic Innovation in Ceramic Technology." *Journal of Archaeological Science* 57: 207–222. https://doi.org/10.1016/j.jas.2015.01.021.

Carlevato, D. 1988. "Late Ceramics From Pucara, Peru: An Indicator of Changing Site Function." *Expedition* 30, no. 3: 39–45.

Choi, J., S. Yang, W. D. Gilstrap, D. Cho, and M. D. Glascock. 2017. "Compositional Analysis of Ceramics From Goguryeo Fortified Sites in Central Korea." *Archaeometry* 59, no. 6: 1018–1033. https://doi.org/10.1111/arcm.12293.

Cocker, M. 2018. *Summary for the Mineral Information Package for the Ghunday-Achin Magnesite and Talc Area of Interest*. USGS.

Downes, J., ed. 2012. *ScARF 2012 Panel Report: Chalcolithic and Bronze Age Scotland*. Society of Antiquaries of Scotland.

Duistermaat, K. 2017. "What's Cooking at the Dunnu? Thoughts on an Exotic, Steatite-Tempered Pottery Cauldron in the "Kitchen" of Grand Vizier Ili-Pada at Middle Assyrian Tell Sabi Abyad, Syria." In *From the Four Corners of the Earth. Studies in Iconography and Cultures of the Ancient Near East in Honour of F.A.M. Wiggermann*, edited by D. Kertai and O. Nieuwenhuyse, 45–72. Ugarit-Verlag.

ESCAP. 1995. "Geology and Mineral Resources of Afghanistan." Atlas of Mineral Resources of the ESCAP Region No. 11. United Nations, New York.

14754754, 0, Downloaded from https://onlinelibrary.wiley.com/doi/10.1111/arcm.70203 by CochraneItalia, Wiley Online Library on [09/09/2026]. See the Terms and Conditions (https://onlinelibrary.wiley.com/terms-and-conditions) on Wiley Online Library for rules of use; OA articles are governed by the applicable Creative Commons License

Földvári, M. 2011. *Handbook of Thermogravimetric System of Minerals and Its Use in Geological Practice*. Occasional Papers of the Geological Institute of Hungary. Vol. 213. Hungarian Academy of Sciences.

Gascoigne, A. L. 2013. "Cooking Pots and Choices in the Medieval Middle East." In *Pottery and Social Dynamics in the Mediterranean and Beyond in Medieval and Post-Medieval Times*, edited by J. Bintliff and M. Caroscio, 1–10. Archaeopress.

Gliozzo, E. 2020. "Ceramic Technology: How to Reconstruct the Firing Process." *Archaeological and Anthropological Sciences* 12: 260. https://doi.org/10.1007/s12520-020-01133-y.

Holakooei, P., U. Franke, S. Röhrs, N. Eftekhari, and C. Vaccaro. 2026. "On the Provenance of Stonepaste Bodies of Tiles From Takht-E Soleyman, Northwestern Iran." *Journal of Archaeological Science: Reports* 70: 105646. https://doi.org/10.1016/j.jasrep.2026.105646.

Holakooei, P., B. Rafiei-Alavi, A. Shojaee-Esfahani, et al. 2024. "A Provenance Study on the Ceramics Excavated at the Varzaneh Plain, Central Iran." *Heritage Science* 12: 416. https://doi.org/10.1186/s40494-024-01532-7.

Ikaheimo, J., and R. Panttila. 2002. "Explaining Ceramic Variability: The Case of Two Tempers." *Fennoscandia Archaeologica* 19: 3–11.

Jennings, S. 2018. "Softstone at Siraf." In *Softstone: Approaches to the Study of Chlorite and Calcite Vessels in the Middle East and Central Asia, From Prehistory to the Present*, edited by C. S. Phillips and S. J. Simpson, 207–215. Archaeopress.

Johnson, J. A. 2016. "One Eye Forward, One Eye Back: Multiple Temporalities, Community, and Social Change in the Culture History of the Southern Urals, Russian Federation (2100–1300 BC)." In *Fitful Histories and Unruly Publics*, edited by K. O. Weber, E. Hite, L. Khatchadourian, and A. T. Smith, 56–79. Brill.

Kaiser, T. 1989. "Steatite Tempered Pottery From Selevac, Yugoslavia: A Neolithic Experiment in Ceramic Design." *Archeomaterials* 3, no. 1: 1–10.

Lyons, D., J. Ferguson, D. Harlow, and J. Casey. 2018. "Marginalized Potters and Ceramic Compositional Groups: Neutron Activation Analysis of Contemporary Pottery From Tigray, Northern Highland Ethiopia." *African Archaeological Review* 35: 567–595. https://doi.org/10.1007/s10437-018-9311-5.

Maritan, L. 2024. "Ceramics: Chemical and Petrographic Analysis." In *Encyclopedia of Archaeology*, edited by E. Nikita and T. Rehren, vol. 2B, 386–397. Academic Press. https://doi.org/10.1016/B978-0-323-90799-6.00020-3.

Maritan, L., G. Ganzarolli, F. Antonelli, et al. 2021. "What Kind of Calcite? Disclosing the Origin of Sparry Calcite Temper in Ancient Ceramics." *Journal of Archaeological Science* 129: 105358.

Maritan, L., L. Nodari, C. Mazzoli, A. Milano, and U. Russo. 2006. "Influence of Firing Conditions on Ceramic Products: Experimental Study on Clay Rich in Organic Matter." *Applied Clay Science* 31: 1–15.

Maritan, L., R. Piovesan, M. C. Dalconi, et al. 2018. "Looking Like Gold: Chlorite and Talc Transformation in the Golden-Slip Ware Production (Swat Valley, North-Western Pakistan)." *Minerals* 8, no. 5: 200. https://doi.org/10.3390/min8050200.

Neighbour, T., T. Cowie, S. Boardman, and C. Rushe. 1998. "Excavation of a Presumed Round House and Associated Features at Priesthill Farm, Near Delny, Ross and Cromarty District, Highland Region, 1993." *Northern Studies* 33: 67–91.

Nodari, L., E. Marcuz, L. Maritan, C. Mazzoli, and U. Russo. 2007. "Hematite Nucleation and Growth in the Firing of Carbonate-Rich Clay for Pottery Production." *Journal of the European Ceramic Society* 27: 4665–4673.

Orris, G. J., and J. D. Bliss. 2002. "Mine and Mineral Occurrences of Afghanistan." Open-File Report 2002–110. US Geological Survey. https://doi.org/10.3133/ofr02110.

Ownby, M. F., C. L. Ownby, and E. J. Miksa. 2004. "Use of Scanning Electron Microscopy to Characterize Schist as a Temper in Hohokam Pottery." *Journal of Archaeological Science* 31, no. 1: 31–38. https://doi.org/10.1016/j.jas.2003.06.001.

Paiman, Z. 2013. *Tepe Narenj à Caboul: Le Tepe Narenj ou l'art bouddhique à Caboul au temps des incursions musulmanes. Chronologie, bâtiments, céramiques et monnaies*. Publ. Inst. Civilis. Indienne. Collège de France, de Boccard.

Paiman, Z., and A. Filigensi. 2019. "Etude préliminaire de quelques aménagements du monastère bouddhique de Qol-E-Tut." *Newsletter di Archeologia CISA* 10: 287–319.

Paiman, Z., and J. Houal. 2023. "Pottery Studies in Kabul (Afghanistan) and Its Region From 100 BCE to 1000 CE." *Archaeological Research in Asia* 34: 1–20.

Porter, A. 2018. "The Distribution and Provenance of Ancient South Arabian Steatite-Tempered Pottery: A Thin-Section Analysis." In *Softstone: Approaches to the Study of Chlorite and Calcite Vessels in the Middle East and Central Asia, From Prehistory to the Present*, edited by C. S. Phillips and S. J. Simpson, 136–166. Archaeopress.

Potts, D. T., K. Radner, A. Squitieri, et al. 2018. "Gird-I Rostam 2018: Preliminary Report on the First Season of Excavations by the Joint Kurdish-German-American Team." *Jaarbericht "Ex Oriente Lux"* 47: 91–127.

Quinn, P. 2022. *Thin Section Petrography, Geochemistry and Scanning Electron Microscopy of Archaeological Ceramics*. Archaeopress. https://doi.org/10.2307/j.ctv2nwq8x4.

Rafiei-Alavi, B., A. Shojaee-Esfahani, A. A. Vahdati, et al. forthcoming. "New Archaeological Field Research at Bala Hissar of Kabul in 2022, 2023, and 2024." European Association for South Asian Archaeology and Art, Leipzig.

Reedy, C. L., P. B. Vandiver, T. He, and Y. Xu. 2017. "Talc-Rich Black Tibetan Pottery of Derge County, Sichuan Province, China." *MRS Advances* 2: 1943–1968. https://doi.org/10.1557/adv.2017.287.

Renaud, K. M. 2024. "The Mineral Industry of Afghanistan." 2020–2021 Minerals Yearbook, Afghanistan [Advance Release] USGS.

Riccardi, M. P., B. Messiga, and P. Duminuco. 1999. "An Approach to Dynamics of Clay Firing." *Applied Clay Science* 15, no. 3–4: 393–409. https://doi.org/10.1016/S0169-1317(99)00032-0.

Steudel, A., R. Kleeberg, C. Bender Koch, F. Friedrich, and K. Emmerich. 2016. "Thermal Behavior of Chlorites of the Clinochlore-Chamosite Solid Solution Series: Oxidation of Structural Iron, Hydrogen Release and Dehydroxylation." *Applied Clay Science* 132–133: 626–634.

Sutphin, D. M., G. J. Orris, and J. D. Bliss. 2007. "Ultramafic-Hosted Talc-Magnesite." In *Preliminary Non-Fuel Mineral Resource Assessment of Afghanistan*, edited by S. Peters, S. Ludington, G. Orris, et al. Afghanistan Geological Survey/U.S. Agency for International Development.

Tahir, M., A. Imai, R. Takahashi, and S. Yano. 2018. "Ore Genesis and Geochemical Characteristics of Carbonate-Hosted Talc Deposits in Nangarhar Province, Afghanistan." *Resource Geology* 68, no. 4: 352–372. https://doi.org/10.1111/rge.12174.

Takesue, J. 2011. "Prehistory of Okinoshima Rituals." In *Okinoshima Island and Related Sites in the Munakata Region*, 1–46. World Heritage Promotion Committee of Okinoshima.

Tenconi, M., L. Maritan, and C. Mazzoli. 2016. "Textural Changes in Speleothem Inclusions During Firing: A Useful Tool to Estimate Temperature in Speleothem-Bearing Pottery." *Archaeometry* 58, no. 1: 39–53.

Tite, M. S. 1995. "Firing Temperatures Determination: How and Why?" In *The Aim of Laboratory Analyses of Ceramics in Archaeology*. Konferenser, edited by A. Lindahl and O. Stilborg, vol. 34, 37–42. Almqvist and Wiksell International.

14754754, 0, Downloaded from https://onlinelibrary.wiley.com/doi/10.1111/arcm.70203 by CochraneItalia, Wiley Online Library on [09/09/2026]. See the Terms and Conditions (https://onlinelibrary.wiley.com/terms-and-conditions) on Wiley Online Library for rules of use; OA articles are governed by the applicable Creative Commons License

Tomasini, E. P., E. B. Halac, M. Reinoso, E. J. Di Liscia, and M. S. Maier. 2012. "Micro-Raman Spectroscopy of Carbon-Based Black Pigments." *Journal of Raman Specroscopy* 43: 1671–1675. https://doi.org/10.1002/jrs.4159.

Travé Allepuz, E. 2021. "Colour Transformation and Textural Change in Biotite: Some Remarks for the Interpretation of Firing Technology in Greyware Pottery Thin-Sections." *Minerals* 11, no. 4: 428. https://doi.org/10.3390/min11040428.

Wilson, J. G. 1973. "The Addition of Talc and Asbestos to Pot Clay by Past and Present Inhabitants of Karamoja District in Uganda and Adjoining Districts of Kenya." *Man* 8, no. 2: 300–302.

Yousufzai, A., H. Waizy, A. B. Qanit, and Q. Yousufzai. 2020. "Mineralogy and Geochemistry of Talc Deposits in the Khogyani District of the Nangarhar Province, Afghanistan." *Research Reviews* 5, no. 7: 128–138.

Zampierin, D., P. Moita, S. Lischi, M. van Aerde, P. Barrulas, and J. Mirão. 2024. "A Multi-Analytical Approach Applied to Pottery From Oman as a Key to Understanding Ancient Indian Ocean Maritime Trade." *Archaeometry* 66, no. 5: 967–1015. https://doi.org/10.1111/arcm.12949.

Supporting Information

Additional supporting information can be found online in the Supporting Information section. **Table S1:** Specifications of talc-tempered potteries illustrated in Figure S2 recovered from Bala Hissar, Kabul. **Table S2:** Compositional data from the bodies of the potsherds (data in wt% for the major and minor elements expressed as oxides, and ppm for the trace elements) (L.O.I.: loss of ignition). **Table S3:** μ-XRF compositional data from analysing 5 talc crystals in Samples 1–3 (in ppm). **Table S4:** SEM-EDS compositional data from chromite crystals found in the bodies (data are normalised to 100 wt% and Cr# is calculated based on the atomic percent of Cr and Al using Cr/(Cr + Al)). **Table S5:** Mineralogical composition obtained from the XRPD quantitative phase analysis (palygorskite is present in all samples with a quantity lower than 0.5 wt%). **Table S6:** Loss on ignition (LOI) of the samples based on the XRPD and TG data. **Figure S1:** Potsherds selected for study from Bala Hissar archaeological site. **Figure S2:** Photographs of talc-tempered ceramics from Bala Hissar, Kabul, and drawing of the relative object they belong to. **Figure S3:** Correlation of transitional elements Ni, Fe, Zn and Cu in 5 talc crystals in Sample 2 and (bottom right graph) Sample 3. **Figure S4:** X-ray elemental of SEM-EDS collected from the cross-section of the Sample 1. **Figure S5:** XRPD patterns of the Samples 1–6 (from top to bottom). Abbreviations: Cal, calcite; Clc, clinochlore; Dol, dolomite; Plg, palygorskite; Qz, quartz. The undefined lines are related to Tlc, talc. **Figure S6:** PCA score plot (left) and HCA dendrogram (right) obtained from the XRPD patterns of the samples. **Figure S7:** Raman spectra collected from the Sample 1, which shows the major occurrence of talc and carbon black. **Data S1:** Supporting information.

14754754, 0, Downloaded from https://onlinelibrary.wiley.com/doi/10.1111/arcm.70203 by Cochraneltalia, Wiley Online Library on [09/09/2026]. See the Terms and Conditions (https://onlinelibrary.wiley.com/terms-and-conditions) on Wiley Online Library for rules of use; OA articles are governed by the applicable Creative Commons License